ELSEVIER

Journal of Fluids and Structures 20 (2005) 949–959

JOURNAL OF FLUIDS AND STRUCTURES

www.elsevier.com/locate/jfs

Performance of flapping foil propulsion

L. Schouveiler[a,*], F.S. Hover[b], M.S. Triantafyllou[b]

[a]*Institut de Recherche sur les Phénomènes Hors Equilibre, Technopôle de Château Gombert, 49 rue F. Joliot Curie, BP 146, 13384 Marseille Cedex 13, France*

[b]*Department of Ocean Engineering, Massachusetts Institute of Technology, Building 5-228, 77 Massachusetts Avenue, Cambridge, MA 02139-4307, USA*

Received 4 August 2004; accepted 5 May 2005

Abstract

The performance of an aquatic propulsion system inspired from the thunniform swimming mode is experimentally studied. This consists of generating the propulsive force with a foil undergoing a harmonic flapping which is a combination of a heave translation and a pitch rotation. Experiments are performed at a fixed value of the Reynolds number and of the heave amplitude. The effects of variations of the Strouhal number and of the maximum angle of attack on the thrust force and on the hydromechanical efficiency are investigated. Systematic measurements of the fluid loading show a peak of efficiency of more than 70% for optimal combinations of the parameters. Moreover, a parameter range is identified where efficiency and high thrust conditions are achieved together, as required for use as a propulsion system. When performing experiments on foils undergoing nonsymmetrical flapping, we also observe the maneuvering capacity of such a biomimetic system.

Keywords: Propulsion; Flapping foil

1. Introduction

"About 10^9 years of animal evolution in an aqueous environment … have inevitably produced rather refined means of generating fast movement at low energy cost" (Lighthill, 1969). In his seminal works, Lighthill suggests that a biomimetic design device for aquatic propulsion could be an efficient alternative to the conventional screw propellers.

Most fish generate propulsive force by passing a curvature wave backwards along their body. Depending on the envelope shape of this bending wave, different modes can be distinguished: when the amplitude is large along the whole body, the swimming is of undulatory type and is called anguilliform; if the undulations are confined in the posterior part of the body the swimming is said to be carangiform. Ultimately, when the amplitude is significant only at the tail, the swimming is oscillatory. In this mode, the thrust is primarily generated by the horizontal tail flapping of marine mammals, like whales or dolphins, or by the oscillations of the vertical caudal fin for fishes like sharks or tunas. This family of swimmers, referred to as thunniform, is characterized by a streamlined rigid body, a crescent moon-shaped tail attached to the trunk and a strongly reduced cross-section at the peduncle that attaches the tail to the body, to minimize recoil (Lighthill, 1969). An extensive review on the fish swimming modes can be found in Sfakiotakis et al. (1999).

*Corresponding author.
E-mail address: lionel.schouveiler@irphe.univ-mrs.fr (L. Schouveiler).

0889-9746/$ - see front matter © 2005 Elsevier Ltd. All rights reserved.
doi:10.1016/j.jfluidstructs.2005.05.009

The thunniform swimming mode is known as the most efficient for fast swimming (Lighthill, 1970). For instance, Bose and Lien (1989) estimated that the maximum hydromechanical efficiency of a whale is about 85%. In the present experimental study, we are interested in the study of the propulsive performances of a flapping foil with a wing-like profile. The flapping consists of a combination of heaving and pitching motions which mimic the tail oscillations of thunniform swimmers.

For such propulsive systems, the mechanism of thrust production is based on the jet reaction principle. In fact, under appropriate kinematical conditions, the time-averaged flow downstream of a flapping foil is jet-like and thus is indicative of a net thrust on the foil. Associated to the thrust-producing flapping, the foil wake is constituted of alternate shed vortices similar to the well-known von Kármán vortex street behind elongated bodies except that the vorticity is reversed. Experimental evidence of the generation of thrust has been given, for instance, by Koochesfahani (1989) for a foil pitching sinusoidally about one of its axes, by Lai and Platzer (1999) for a foil oscillated in heave, and by Freymuth (1990), Anderson et al. (1998) or more recently by Read et al. (2003) for a foil harmonically oscillated in a combination of heave and pitch, hereafter referred to as a flapping motion.

The seminal theoretical study on the thunniform swimming is due to Lighthill (1970) who applies the linear two-dimensional theory of oscillating airfoils [see, e.g., Kármán and Sears (1938)]. This theory based on the acceleration potential considers a foil of infinite aspect ratio (span on chord ratio) oscillating in an inviscid incompressible flow. According to this theory, the thrust force results on the one hand from the leading edge suction effect and on the other hand from the component onto the direction of the displacement of the force normal to the foil. The latter results from the difference of pressure between the two sides of the foil and the leading edge suction is due to the reduced pressure associated with the fast flow around the rounded leading edge. Extensions of Lighthill's theory to large amplitude flapping and taking into account three-dimensional effects have been developed in Chopra (1976) and Chopra (1974), respectively.

The present study is devoted to flapping foil experiments where three-dimensional effects have been limited by the use of a specific device at the foil ends. Experimental details are given in Section 2, where the setup and the investigation methods are described. Then, and before concluding, we present the results (in Section 3) which are compared with the Lighthill's theory. They include flow visualization, measurements of the maneuvering capability and of the propulsive performance of the flapping foil system. The latter confirm previous measurements by Read et al. (2003). In the present paper, they are compared with theoretical results resulting from the Lighthill's analysis. Conclusions are given in Section 4.

2. Experimental details

2.1. Experimental set-up

Experiments were performed at the MIT Tow Tank. This facility consists in a free surface container of still water. It is 30 m long, 2.6 m wide and has a 1.2 m water depth. A rectangular symmetric foil of constant NACA0012 section, with a span s of 0.6 m and a chord c of 0.1 m, was used. An axis was inserted at each end of the foil, on the symmetry plane at one-third of the chord from the leading edge. The foil was supported by these axes on an inverted U-frame at a mean height corresponding to the mid-depth of the tank. The U-frame was attached to a carriage located above the free surface of the water and can be translated at an adjustable velocity U. The working length of the carriage run is 18 m. The three-dimensional effects are limited by two circular endplates of 0.35 m of diameter mounted at each end of the foil. While it was horizontally towed at the velocity U, the foil was oscillated at a frequency ω in a combination of heave (vertical displacement) and pitch (rotation around the foil axis) motion as displayed in Fig. 1(a). The three motions are driven by three separate motors, controlled by a computer.

We denote by $y(t)$ the instantaneous vertical position of the foil axis (or heave position) positively counted upwards and with the zero corresponding to the mid-depth of the foil in the tank (Fig. 1). The pitch angle $\theta(t)$ is the instantaneous angle between the towing velocity U and the foil chord. In the present study, the foil motion is limited to the simple harmonic flapping defined by

$$y(t) = y_0 \sin(wt) \tag{1}$$

and

$$q(t) = q_0 \sin(wt + y), \tag{2}$$

where ψ is the phase angle between heave and pitch.

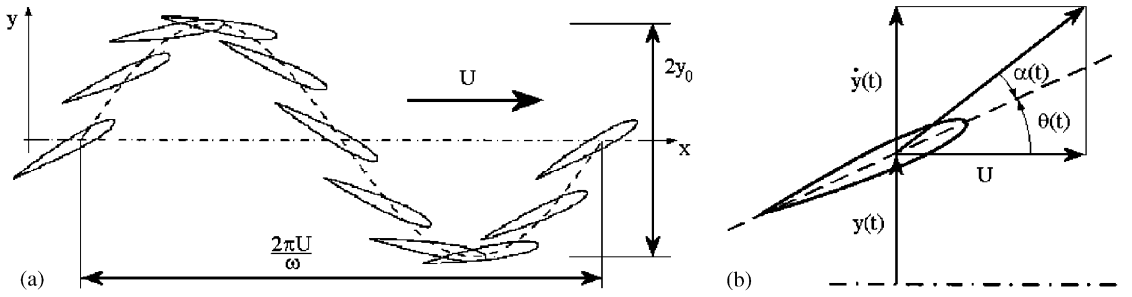

Fig. 1. (a) Kinematical parameters of the foil motion and (b) definition of the angle of attack $\alpha(t)$.

The velocity of the fluid relative to the foil results on the one hand from the horizontal towing velocity U and on the other hand from the vertical heave velocity $\dot{y}(t) = \mathrm{d}y/\mathrm{d}t$. Therefore, the instantaneous angle of attack $\alpha(t)$ of the foil, i.e., the angle between the effective flow velocity and the chord, is given by

$$\alpha(t) = \theta(t) - \tan^{-1}\left(\frac{\dot{y}}{U}\right), \tag{3}$$

as described in Fig. 1(b).

During a run, the vertical position $y(t)$, the pitch angle $\theta(t)$, the net horizontal and vertical (or side) forces exerted on the foil, $F_x(t)$ and $F_y(t)$, and the torque $M(t)$ around the pitch rotation axis were simultaneously recorded. The acquisition frequency was 200 Hz. The two components of the net force and of the torque were measured by means of a piezoelectric load cell mounted between the foil axis and the support U-frame. This cell was regularly calibrated. The heave position is measured using an optical encoder and the pitch angle with a variable resistance device.

For the visualization of the vortices shed in the wake, the foil was initially painted with a dye and the wake is illuminated at mid-span by a light sheet of few centimeters of thickness and parallel to the foil displacement. The light was mounted on the carriage. The images were captured with a numerical camera, through the tank glass sidewall.

2.2. Parameters and procedure

The aspect ratio (ratio of the span on the chord s/c) of the foil used in this study is equal to 6 and the pitch rotation axis is located at one-third of chord length c from the leading edge. The other nondimensional parameters for the foil flapping motion are the Reynolds number $\mathrm{Re} = Uc/\nu$, where ν is kinematical viscosity of the fluid, the heave amplitude normalized with the chord y_0/c, the amplitude θ_0 of the pitch rotation, the phase angle ψ between heave and pitch and the Strouhal number defined by

$$\mathrm{St} = \frac{2y_0\omega}{2\pi U}, \tag{4}$$

where $2y_0$ is considered here as estimated length of the wake width. Some authors prefer the use of the reduced frequency $(2c\omega)/(2U)$ to the Strouhal number, but this later has been shown to be more suitable for the propulsion studies [see discussions, e.g., in Triantafyllou et al. (1991) or Ramamurti and Sandberg (2001)].

For the results reported in this paper, the towing velocity U was set to $0.4\,\mathrm{m\,s^{-1}}$, resulting in a Reynolds number Re of 40 000, and the amplitude of the heave motion y_0 was set to $0.75 \times c$ (i.e., 7.5×10^{-2} m). Moreover, we limit our investigation to a phase difference ψ between the heaving and pitching motions equal to 90° which corresponds to the optimum for the propulsion as reported in previous experimental (Anderson et al., 1998; Read et al., 2003) or numerical (Isogai et al., 1999; Ramamurti and Sandberg, 2001) studies. Then the procedure consisted to fix the Strouhal number St, therefore the frequency ω, and the maximum of the angle of attack $\alpha_{\max}$, defining then θ_0. St was then varied between 0.10 and 0.45 by a step of 0.05 and $\alpha_{\max}$ from 10° to 35° by a step of 5°. As discussed in Read et al. (2003), θ_0 determined by this way is not unique. Actually, two solutions exist over a large part of the parameters St and $\alpha_{\max}$: one corresponding to a drag-generating flapping and the other to a thrust-producing flapping. Only the latter is considered in the present study.

3. Results

3.1. Visualization

Qualitative features of the vortical patterns in the wake of the foil are first examined by means of flow visualization. It should be pointed out that the combinations of the parameters St and α_{max} leading to a value of the pitch amplitude θ_0 equal to or less than zero, including in particular the cases of drag-generating motion (see next section), are mainly characterized by a strong flow separation giving rise to generation of vortices at the leading edge. This could be seen by the direct observations of the dye pattern but, due to the nontransparent U-frame, we have not been able to obtain clear pictures of the phenomenon.

For the thrust-producing situations, the procedure described in the previous section which consists of imposing a harmonic flapping defined by relations (1) and (2) gives rise to different kinds of temporal evolutions for the angle of attack $\alpha(t)$ depending on the values of St and α_{max}. More precisely, at a given value of the maximum of the angle of attack α_{max} we observe, for low values of the Strouhal number St, a cosine-type profile with two extrema per cycle [Fig. 2(a)]: one maximum and one minimum, alternately, when the foil is at the mid-height positions $y = 0$. As St is increased [Figs. 2(b) and (c)], $\alpha(t)$ differs more and more from this harmonic behavior. We first note flattened extrema as in Fig. 2(b), then for higher St each extremum splits, resulting in an angle of attack profile with two maxima and two minima per cycle [Fig. 2(c)]. The appearance of these supplementary extrema occurs at higher values of St as α_{max} is increased. Hover et al. (2004) have recently tested a different experimental procedure that consists of imposing the shape of the angle of attack profile; they considered square, symmetric sawtooth and cosine functions. Their results will be shortly discussed in Section 3.2.

Visualizations show that this change in the evolution of the angle of attack is associated with a change in the pattern of the vortices shed in the foil wake. This is illustrated in Fig. 3 for two combinations of the parameters St and α_{max}.

When the angle of attack behaves almost like a cosine as in Fig. 2(a), visualizations show that two vortices of opposite sign are shed per cycle [Fig. 3(a)]. This case looks like the well-known von Kármán vortex street behind a stationary cylinder maintained in a flow perpendicular to its axis, but with reversed sense of rotation of the vortices. In contrast, for angle of attack variations that strongly differ from a harmonic behavior, as in Fig. 2(c), a train of two or three corotating vortices is generated during half of the flapping cycle (corresponding, e.g., to the upward heave motion) and a train of corotating vortices, with opposite direction of rotation, during the second half. The visualizations show that the corotating vortices merge as they are advected downstream (relative to the foil) and form large scale vortices [see Fig. 3(b)]. Thus, in both cases, a street of alternate vortices is created in the far wake, as illustrated in Figs. 3(a) and (b). These vortices induce a streamwise unsteady velocity component in the wake flow. The time-averaged velocity profile is of the jet-type, indicative of a thrust-producing foil motion contrary to wake-type profiles which are associated with a net drag.

3.2. Force measurements

Besides these qualitative descriptions, we have also quantified the performance of the flapping foil for propulsion by means of forces and torque measurements. We present in Fig. 4 an example of the simultaneous time recordings of the two force components $F_x(t)$ and $F_y(t)$, and of the torque $M(t)$, together with the heave $y(t)$ and pitch angle $\theta(t)$. During this run θ_0 was positive, the Strouhal number St and the maximum α_{max} of the angle of attack were fixed to 0.30° and 20°, respectively. These values give an angular frequency $\omega = 5.03\,\mathrm{rad\,s^{-1}}$, or equivalently a period of about 1.25 s, and a pitch angle amplitude θ_0 slightly above 23°. As for all the experiments in the present study, the heave position $y(t)$ of the foil evolves in the range $\pm 7.5 \times 10^{-2}$ m corresponding to a heave amplitude of $\frac{3}{4}$ of the chord c. We can note that, while the torque M and the vertical force F_y exerted on the foil are alternatively positive and negative, the horizontal force component F_x always points in the same direction during the upward and downward foil heave motion. It results that the frequency of $F_x(t)$ is twice that of the flapping. The sign of F_x depends on the flapping kinematic. In the present case, F_x is positive, i.e., propulsive. In a drag-producing case, the net horizontal force would be negative, i.e., opposite to the foil displacement.

The maxima of F_x and extrema of F_y are reached when the heave velocity $\dot{y}$ together with the pitch angle θ are maximum: $y = 0$ and $\theta = \theta_0$. The two force components are zero when the heave velocity vanishes: $y = \pm y_0$ and $\theta = 0$. In the example of Fig. 4, the peak values for F_x and F_y are about 5.2 and 9.8 N, respectively; and the torque around the pitch axis M evolves in the range ± 0.1 N m.

To examine the propulsive performance we are interested in the time-averaged forces. The average values $\bar{F}_x$ and $\bar{F}_y$ are computed on a number n of flapping periods $T = 2\pi/\omega$. At the towing velocity that we considered here, the number

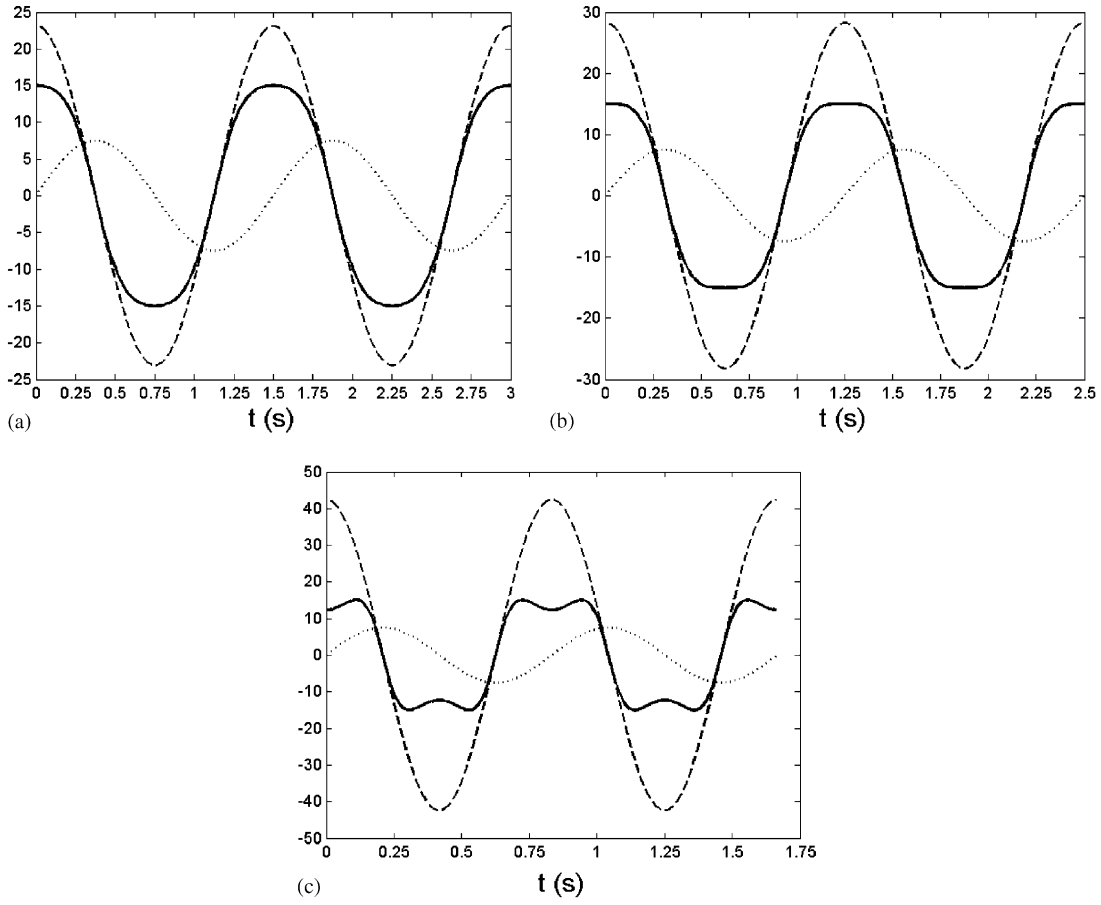

Fig. 2. Temporal evolutions of heave position $y(t)$ (dotted line, in cm), pitch angle $\theta(t)$ (dashed line, in deg) and resulting angle of attack $\alpha(t)$ (bold line, in deg) for $\alpha_{max} = 15^\circ$ and (a) St = 0.25, (b) St = 0.30, (c) St = 0.45.

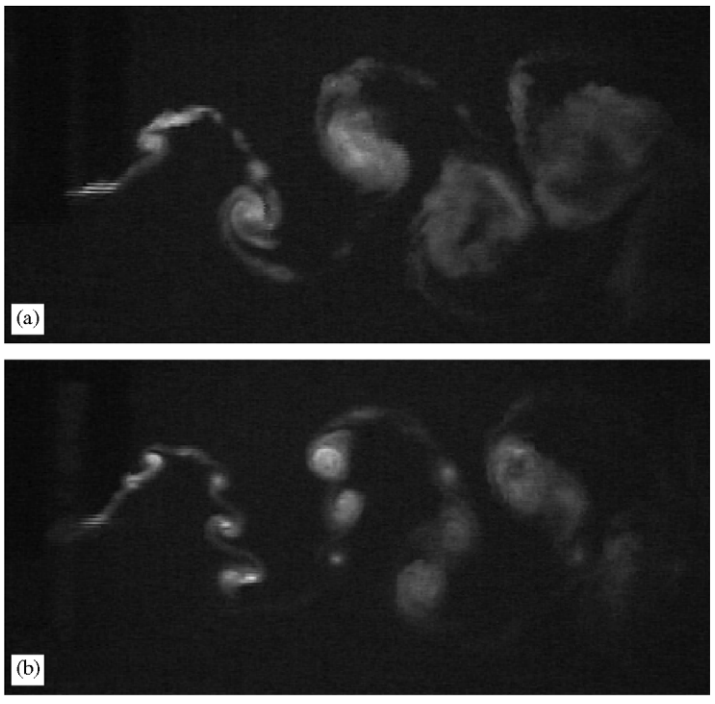

Fig. 3. Vortical pattern visualized in the foil wake for (a) St = 0.45, $\alpha_{max} = 30^\circ$ and (b) St = 0.45, $\alpha_{max} = 20^\circ$. Foil towed from right to left. The visible distance is horizontally approximately of 8 chord lengths and vertically of 4 chord lengths, the foil is at mid-height with the leading edge at the left edge of the pictures.

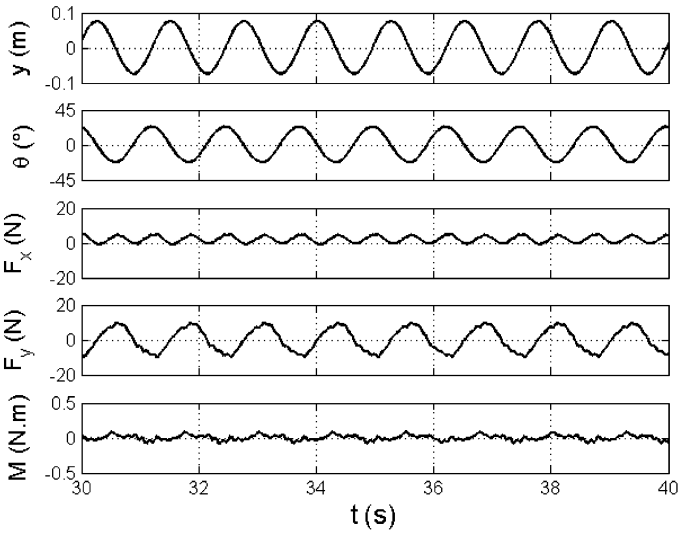

Fig. 4. From the top to the bottom: time recordings of the instantaneous heave and pitch position, of the horizontal and vertical force component and of the torque around the pitching axis for St = 0.30 and $\alpha_{max} = 20^\circ$.

n of periods per run varies from 10 at St = 0.10 to 45 for St = 0.45. The time-averaged mechanical power $\bar{P}$ required to activate the foil, or input power, is calculated by

$$\bar{P} = \frac{1}{nT}\int_0^{nT} F_y(t)\dot{y}(t) + M(t)\dot{\theta}(t)\mathrm{d}t. \tag{5}$$

These mean quantities are expressed in the following in terms of the nondimensional mean force coefficients C_x, C_y and power coefficient C_P defined by

$$\bar{F}_x = \tfrac{1}{2}\rho U^2 csC_x, \tag{6}$$

$$\bar{F}_y = \tfrac{1}{2}\rho U^2 csC_y \tag{7}$$

and

$$\bar{P} = \tfrac{1}{2}\rho U^3 csC_P, \tag{8}$$

where ρ is the water density, c and s are the chord and the span of the foil, respectively. Although we do not consider the effects of variation of the Reynolds number Re here, it should be pointed out that these coefficients usually depend on this parameter. For the thrust-producing situations $C_x > 0$, we define the hydromechanical propulsive efficiency η as being the ratio of the output power $\bar{F}_x U$ on the input power $\bar{P}$. From relations (6) and (8), η is given by

$$\eta = \frac{\bar{F}_x U}{\bar{P}} = \frac{C_x}{C_P} \tag{9}$$

and, owing to the energy loss (mainly due to the vortices shed in the wake), η is less than unity. For the example of Fig. 4 we find $C_y = 0$, $C_x = 0.45$ and an efficiency η of about 61%.

Due to the up-and-down symmetry of the foil profile and of the flapping motion, the side force varies symmetrically about zero (Fig. 4) in such a way that the time average value $\bar{F}_y$ and therefore the force coefficient C_y are always zero. The experimental results for the horizontal force coefficient C_x and for the efficiency η are presented in Fig. 5. These data correspond to the parameter range: $0.10 \leqslant \mathrm{St} \leqslant 0.45$, $10^\circ \leqslant \alpha_{max} \leqslant 35^\circ$ and Re = 40 000. The contour plots for C_x and η are deduced from the load measurements performed at the points of the (St, α_{max})-plane corresponding to the intersection points of the displayed grid. These measurements were performed up to 20 times to check the repeatability and to estimate the experimental uncertainty. We found that C_x and η are experimentally determined with an uncertainty of less than 4% and 7%, respectively.

The main features of the propulsive performance of the flapping foil in the parameter range explored during the present study are shown in Fig. 5; they are detailed in the following.

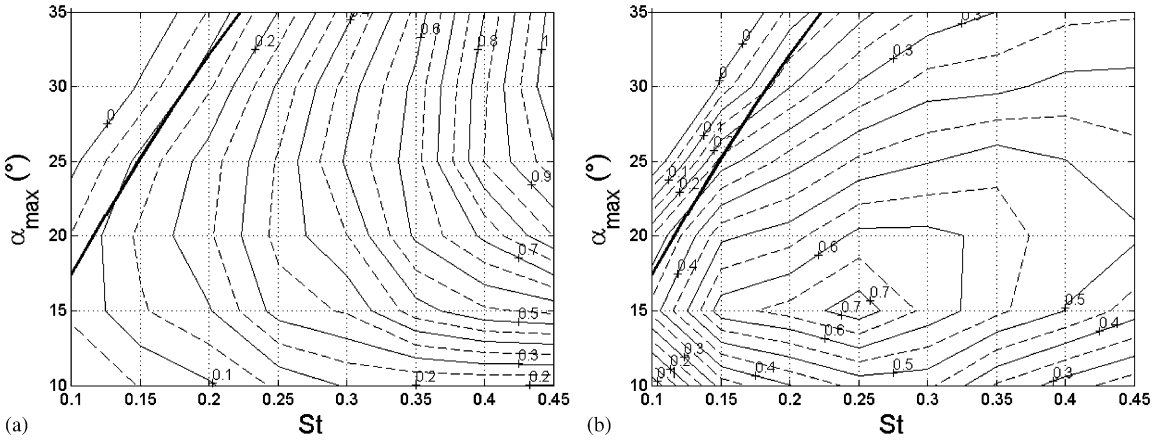

Fig. 5. (a) Force coefficient C_x and (b) efficiency η as deduced from the measurements with respect to the Strouhal number St and to the maximum of the angle of attack α_{max}; bold line: $\theta_0 = 0$.

In Fig. 5(a) we can see that the thrust force coefficient C_x increased with the Strouhal number St while it first rises then decreases when the maximum of the angle of attack α_{max} is increased. For increasing St, we observe a continuous evolution from a drag-producing ($C_x<0$ and $\eta<0$) to a thrust-producing motion ($C_x>0$ and $\eta>0$). Thus in the parameter region under consideration, negative values of the mean horizontal force C_x have been obtained for $\alpha_{max} \geqslant 25^\circ$ and low St (upper left side area). The bold line in Fig. 5 corresponds to this condition, that is, to a pure heave motion of the foil. When $\theta_0 = 0$, the thrust component due to the difference of pressure between the two sides of the foil is obviously zero because the resulting force is perpendicular to the displacement during the whole flapping cycle. This component is even opposite to the foil displacement, thus giving a drag component, for $\theta_0<0$, i.e., to the left of the thick line. But thanks to the leading-edge suction component to the thrust force, it is possible to get a positive mean horizontal force $C_x>0$ for values of θ_0 less than zero. In agreement, the boundary between thrust- to drag-producing motion, corresponding to the level curves $C_x = 0$ and $\eta = 0$ in Fig. 5, therefore appears to the left of the ($\theta_0 = 0$)-curve for lower St values. For a foil with fore-and-aft symmetry this leading-edge suction component vanishes as recently evidenced by the numerical simulations of Guglielmini and Blondeaux (2004) for a foil with an elliptical profile (rather than a wing-like profile).

The maximum of the thrust is reached at a value of α_{max} which evolves from 15° for St = 0.1 to 30° for St = 0.45. And the maximum thrust coefficient C_x we have measured is of 1.05 ± 0.04 at (St = 0.45, $\alpha_{max} = 30^\circ$) where the hydromechanical efficiency is $\eta = 0.42 \pm 0.025$.

The efficiency presents a well-defined unique peak in the considered parameter range [see Fig. 5(b)]. The highest value of the efficiency has been measured for St = 0.25 and $\alpha_{max} = 15^\circ$, and is $\eta = 0.73 \pm 0.04$. It is associated with a moderate thrust coefficient $C_x = 0.32 \pm 0.01$. It is noteworthy that efficiency is maximized at a St value of 0.25 corresponding to the instability mode of maximum growth rate, deduced from the stability analysis of experimental velocity profiles behind a flapping foil by Triantafyllou et al. (1991). In Section 3.1 we noted that $\alpha(t)$ differs more and more from a cosine-type behavior as St is increased [see Fig. 2]. In the contour plot of Fig. 5(b), maxima of the efficiency η at fixed α_{max} can be distinguished for $\alpha_{max} = 15^\circ$, 20° and 25°; they respectively occur for values of St equal to 0.25, between 0.25 and 0.30, and equal to 0.35. These maxima of η occur for combinations of St and α_{max} resulting in an angle of attack profiles of cosine-type [as in Fig. 2(a)]. This is in agreement with the recent experiments of Hover et al. (2004) that consisted of measuring the propulsive performance of a foil oscillating with an imposed angle of attack profile; they report that the most efficient situation is achieved with a cosine profile (although highest thrusts are found with a sawtooth profile).

For use as a propulsion system, the conditions of high efficiency together with high thrust are required. These two conditions are not encountered outside of the parameter range we explored for the present study. In fact, if Fig. 5(a) shows that higher thrust can be expected when increasing the Strouhal number and/or the maximum of the angle of attack, these high thrusts would be associated with low efficiency: no more than 40% [see Fig. 5(b)]. This is the reason for limiting our study to the parameter range considered, where a large plateau of efficiency higher than 0.5, including a region of thrust coefficient superior to 0.8, exists. This parameter domain includes the maximum of efficiency for the considered Reynolds number and the condition of high thrust together with high efficiency.

The experimental values of the force coefficient C_x and of the hydromechanical propulsive efficiency η are plotted as function of the Strouhal number St in Fig. 6, together with the analytical results of Lighthill (1970). In the interests of brevity, only two values of α_{max}, namely, 15° and 30°, are considered for this comparison. The solid and dotted lines correspond to the theoretical results obtained using Lighthill's analysis adapted to the parameters of the present experimental study. The solid lines represent the total thrust and the dotted lines show the part due to the leading edge suction. The crossings between the dotted and the solid lines correspond to the condition $\theta_0 = 0$ where the thrust is completely due to the leading edge suction. For negative values of θ_0, that is, on the left of the crossing point, the force normal to the foil surface is obviously negative, and a positive thrust results from a strong leading edge suction. Although some qualitative features (as the increase of the C_x with St and the existence of a maximum of η when St is varied at fixed values of α_{max}) are correctly described by the analysis, Fig. 6 shows that the two-dimensional unsteady wing theory adapted by Lighthill overestimates the thrust coefficient and the efficiency as well. The discrepancy may be interpreted because of the limiting hypotheses of the theory. For instance, the net thrust is overestimated because of a viscous drag on the foil (neglected by the inviscid theory) which is nonzero although it is small for the high value of the Reynolds number we consider (40 000). In the same manner, the streamwise vorticity generated at the foil ends and neglected in the two-dimensional analysis can decrease the performance of the foil. Moreover, the validity of the theory is limited to low amplitude motion because it cannot take into account flow separation at the leading edge. This phenomenon is known to occur at an angle of attack of about 15° for a static NACA 0012 airfoil and is slightly delayed by unsteady effects for a flapping foil [see, e.g., the recent numerical study of Akbari and Price (2003)]. Anderson et al. (1998) report that leading edge separation becomes more important, and that the leading edge vortex becomes stronger,

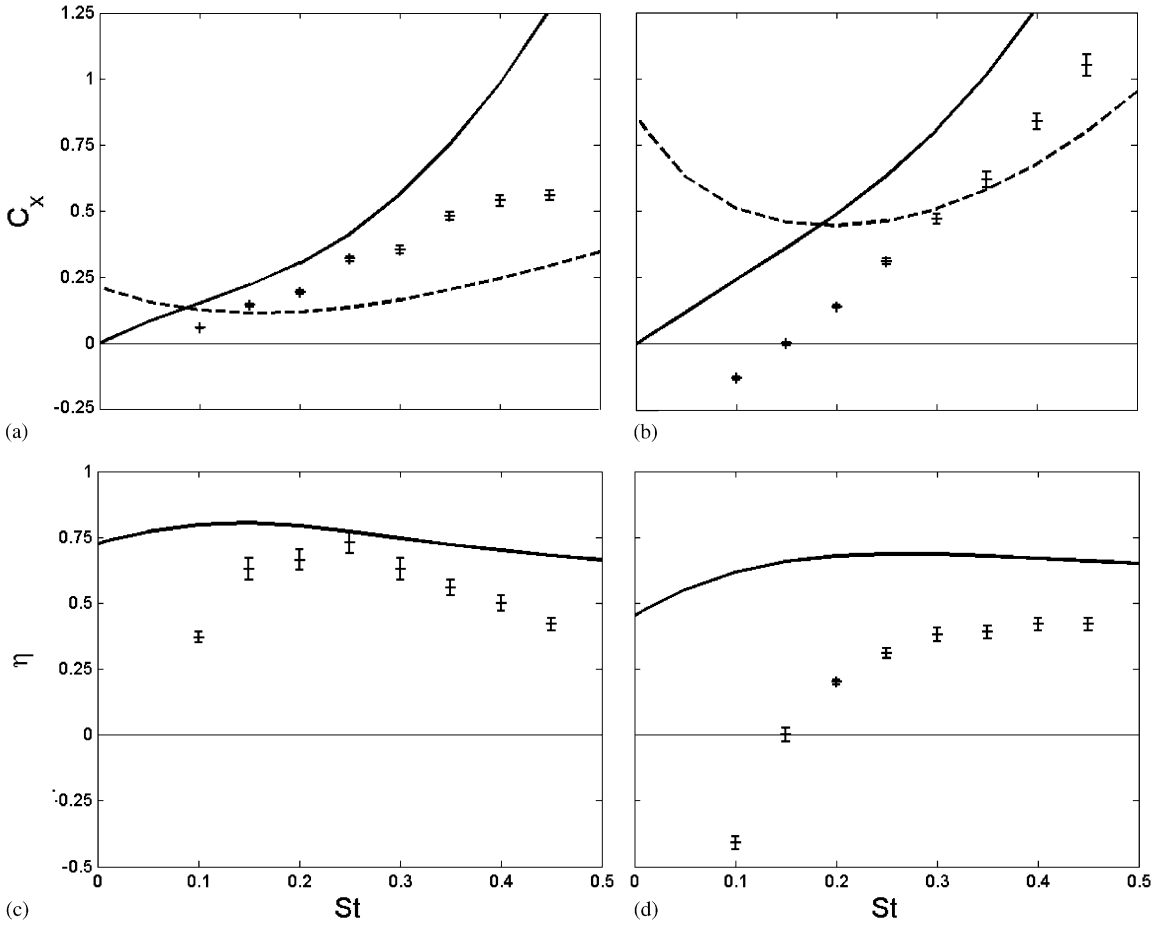

Fig. 6. (a,b) Force coefficient C_x and (c,d) efficiency η as function of the Strouhal number St; for (a,c) $\alpha_{max} = 15°$, and for (b,d) $\alpha_{max} = 30°$; +, experimental data; —, theoretical data;- - -, part of C_x due to the leading edge suction effect as predicted by the theory.

when the maximum angle of attack or Strouhal number is increased. The discrepancy in the thrust and also in the input power leads to an overestimate and a shift of the maximal experimental efficiency towards higher Strouhal number, when compared to Lighthill's theory (Figs. 6(c) and (d)).

Because a strong reduction of the suction force component could result from a separation of the flow at the leading edge, Lighthill (1970) points out that the use of the flapping foil propulsion when this component is important, should be avoided. The same conclusion has been achieved by Isogai et al. (1999) by means of numerical simulations, who report the rapid efficiency decrease with the occurrence of flow separation. On the contrary, the experiments of Anderson et al. (1998) conclude that, in some cases, constructive interactions of the leading and the trailing edge vortices may lead to an improvement of the propulsive performances.

3.3. Nonsymmetrical flapping

Time recordings of loads exerted on the foil (see, e.g., Fig. 4) show that the flapping of the foil generates, in addition to the horizontal force F_x, a vertical force component F_y. The peak value of this side force F_y can be much larger than the propulsive force F_x. It is approximately twice that of the example of Fig. 4 where $\mathrm{St} = 0.30$ and $\alpha_{\max} = 20^\circ$. But due to the symmetry of the foil profile and of the foil motion relative to the income flow, the time-averaged side force C_y is zero. Here, we present a simple way to take advantage of this in order to generate a nonzero mean side force useful for maneuvering the propelled vehicle.

For this purpose, the symmetry of the foil motion with respect to the flow is broken by adding a bias angle θ_m to the pitch and consequently to the angle of attack. Therefore, the instantaneous pitch angle may now be written as

$$\theta(t) = \theta_0 \sin(wt + \psi) + \theta_m, \tag{10}$$

meaning that the foil is oscillated with a nonzero mean pitch angle θ_m. During a cycle of nonsymmetrical flapping, the angle of attack $\alpha(t)$ evolves between $(\theta_m + \alpha_{\max})$ and $(\theta_m - \alpha_{\max})$ and therefore gives rise to higher values for the angle of attack than in the case where $\theta_m = 0$ considered before (Section 3.2). As is clearly evidenced in Fig. 7, which can compared to Fig. 4 differing only by the value of θ_m (of 15° and 0°, respectively), a strong side force is created together with a significant decrease of the horizontal force. In the example of Fig. 6 where $\theta_m = 15^\circ$, the maximum values for the instantaneous forces F_y and F_x are, respectively, 19.6 and 3.2 N (while we found 9.8 and 5.2 N, respectively, when $\theta_m = 0$, Fig. 4). The nondimensional time-averaged force coefficients are $C_y = 1.46$ and $C_x = -0.01$ ($C_y = 0$ and $C_x = 0.45$ for $\theta_m = 0$).

Evolution of the horizontal C_x and side C_y force coefficients when the mean pitch angle θ_m is varied from 0° to 45° is plotted in Fig. 8 for $\mathrm{St} = 0.30$ and $\alpha_{\max} = 20^\circ$. We first note the strong increase of the mean side force C_y when θ_m is increased, then it saturates at a value of about 2.1 (for $\alpha_{\max} > 20^\circ$ a slight decrease of C_y was observed when $\theta_m > 35$ or 40°). The horizontal mean force component C_x monotonously decreases with θ_m, and negative values are obtained when $\theta_m \geqslant 15^\circ$, in such a way that there exists a limit value for θ_m between forward $C_x > 0$ and backward $C_x < 0$ horizontal forces and where a pure side force is obtained. Data for other combinations of St and $\alpha_{\max}$, in the range $10^\circ \leqslant \alpha_{\max} \leqslant 35^\circ$, $0.10 \leqslant \mathrm{St} \leqslant 0.45$ and $0^\circ \leqslant \theta_m \leqslant 45^\circ$, show identical trends. The maximum value we measured for C_y is of about 3.2 when $\mathrm{St} = 0.45$, $\alpha_{\max} = 20^\circ$ and $\theta_m = 40^\circ$.

Note that a similar mechanism has been recognized for the high-lift production in insect flight (Ellington et al., 1996). The high side forces are due to a low pressure above the insect wings resulting from the formation of a strong attached leading edge vortex. This flow separation is due to the high angles of attack encountered in the nonsymmetrical flapping motions. Finally, it should be mentioned that in the case of insect flight, this effect is enhanced by the axial (spanwise) flow due to the three-dimensional wing flapping, that consists of two rotations around perpendicular axes rather than a translation plus a rotation as considered in the present study, which tends to stabilize the leading edge vortex.

4. Concluding discussion

The propulsive performance of a harmonically flapping foil has been experimentally studied. In particular, the influences of the Strouhal number and of the maximum angle of attack have been investigated. Extensive measurements show the ability of this biomimetic propeller for efficient propulsion. The production of high thrust together with high efficiency, as required for applications, is shown.

Moreover, we present a simple way to generate a side force which can be useful for the maneuverability of the propelled vehicle. It consists of breaking the symmetry of the foil flapping by the addition of a bias to the pitch angle,

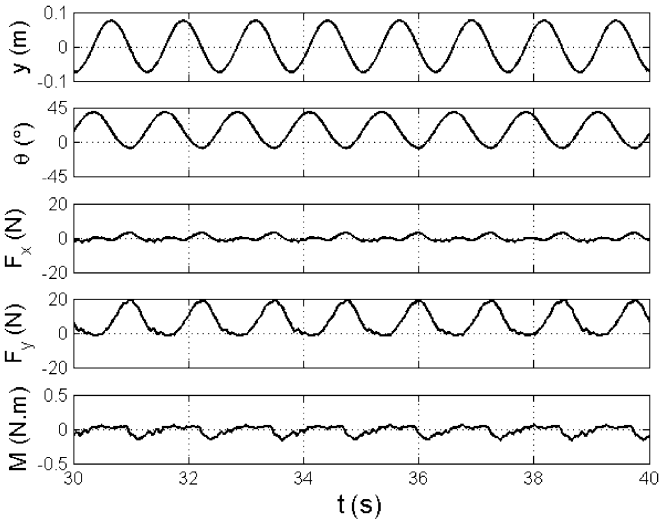

Fig. 7. Same as Fig. 3 with $\theta_m = 15^\circ$.

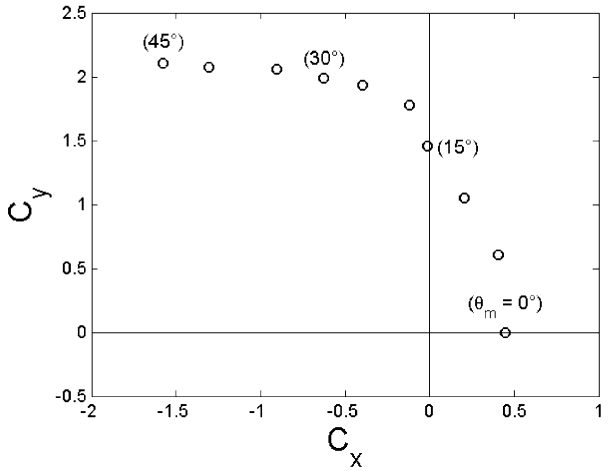

Fig. 8. Evolution of the side force coefficient C_y as function of the horizontal force coefficient C_x when θ_m is varied from 0° to 45° (with an increment of 5°) for St = 0.30 and $\alpha_{max} = 20^\circ$.

and therefore to the angle of attack, and thus requires no modification of the system. Very high side forces have been measured under these conditions.

It should be pointed out that although the propulsion system under investigation in the present study is inspired from the thunniform swimming mode, it alone cannot explain the high performance of such swimming. In fact, it is now known that the thunniform swimmers have developed a mechanism of performance enhancement based on a vorticity control strategy which consists of extracting energy from the vorticity generated along the body and coming onto the flapping caudal fin or tail [see, e.g., the review by Triantafyllou et al. (2000)]. A complete understanding of the swimming energetics requires then to consider the fish as a whole (Zhu et al., 2002).

References

Akbari, M.H., Price, S.J., 2003. Simulation of dynamic stall for a NACA 0012 airfoil using a vortex method. Journal of Fluids and Structures 17, 855–874.

Anderson, J.M., Streitlien, K., Barrett, D.S., Triantafyllou, M.S., 1998. Oscillating foils of high propulsive efficiency. Journal of Fluid Mechanics 360, 41–72.

Bose, N., Lien, J., 1989. Propulsion of a fin whale (*Balaenoptera physalus*): why the fin whale is a fast swimmer. Proceedings of the Royal Society of London B 237, 175–200.

Chopra, M.G., 1974. Hydromechanics of lunate-tail swimming propulsion. Journal of Fluid Mechanics 64, 375–391.

Chopra, M.G., 1976. Large amplitude lunate-tail theory of fish locomotion. Journal of Fluid Mechanics 74, 161–182.

Ellington, C.P., van den Berg, C., Willmott, A.P., Thomas, A.L.R., 1996. Leading-edge vortices in insect flight. Nature 384, 626–630.

Freymuth, P., 1990. Thrust generation by an airfoil in hover modes. Experiments in Fluids 9, 17–24.

Guglielmini, L., Blondeaux, P., 2004. Propulsive efficiency of oscillating foils. European Journal of Mechanics B/Fluids 23, 255–278.

Hover, F.S., Haugsdal, Ø., Triantafyllou, M.S., 2004. Effect of angle of attack profiles in flapping foil propulsion. Journal of Fluids and Structures 19, 37–47.

Isogai, K., Shinmoto, Y., Watanabe, Y., 1999. Effects of dynamic stall on propulsive efficiency and thrust of flapping airfoil. AIAA Journal 37, 1145–1151.

von Kármán, T., Sears, W.R., 1938. Airfoil theory for non-uniform motion. Journal of the Aeronautical Sciences 5, 379–390.

Koochesfahani, M.M., 1989. Vortical patterns in the wake of an oscillating foil. AIAA Journal 27, 1200–1205.

Lai, J.C.S., Platzer, M.F., 1999. Jet characteristics of a plunging airfoil. AIAA Journal 37, 1529–1537.

Lighthill, M.J., 1969. Hydrodynamics of aquatic animal propulsion. Annual Review of Fluid Mechanics 1, 413–446.

Lighthill, M.J., 1970. Aquatic animal propulsion of high hydromechanical efficiency. Journal of Fluid Mechanics 44, 265–301.

Ramamurti, R., Sandberg, W., 2001. Simulation of flow about flapping airfoils using finite element incompressible flow solver. AIAA Journal 39, 253–260.

Read, D.A., Hover, F.S., Triantafyllou, M.S., 2003. Forces on oscillating foils for propulsion and maneuvering. Journal of Fluids and Structures 17, 163–183.

Sfakiotakis, M., Lane, D.M., Davies, J.B.C., 1999. Review of fish swimming modes for aquatic locomotion. IEEE Journal of Oceanic Engineering 24, 237–252.

Triantafyllou, M.S., Triantafyllou, G.S., Gopalkrishnan, R., 1991. Wake mechanics for thrust generation in oscillating foils. Physics of Fluids A 3, 2835–2837.

Triantafyllou, M.S., Triantafyllou, G.S., Yue, D.K.P., 2000. Hydrodynamics of fishlike swimming. Annual Review of Fluid Mechanics 32, 33–53.

Zhu, Q., Wolfgang, M.J., Yue, D.K.P., Triantafyllou, M.S., 2002. Three-dimensional flow structures and vorticity control in fish-like swimming. Journal of Fluid Mechanics 468, 1–28.